



Title	Understanding CO oxidation on the Pt(111) surface based on a reaction route network
Author(s)	Sugiyama, Kanami; Sumiya, Yosuke; Takagi, Makito; Saita, Kenichiro; Maeda, Satoshi
Citation	Physical chemistry chemical physics, 21(26), 14366-14375 https://doi.org/10.1039/c8cp06856a
Issue Date	2019-07-14
Doc URL	http://hdl.handle.net/2115/76606
Type	article (author version)
Additional Information	There are other files related to this item in HUSCAP. Check the above URL.
File Information	01_Phys. Chem. Chem. Phys.21(26)_14366.pdf



[Instructions for use](#)

Understanding CO oxidation on the Pt(111) surface based on a reaction route network

Kanami Sugiyama,^a Yosuke Sumiya,^b Makito Takagi,^a Kenichiro Saita,^{b,} and Satoshi Maeda^{b,c,d,*}*

^a*Graduate School of Chemical Sciences and Engineering, Hokkaido University, Sapporo, 060-8628, Japan.*

^b*Department of Chemistry, Faculty of Science, Hokkaido University, Sapporo, 060-0810, Japan.*

^c*Institute for Chemical Reaction Design and Discovery (WPI-ICReDD), Hokkaido University, Sapporo, 001-0021, Japan.*

^d*Research and Services Division of Materials Data and Integrated System (MaDIS), National Institute for Materials Science (NIMS), Tsukuba, 305-0044, Japan.*

*Authors to whom correspondence should be addressed. E-mail: ksaita@sci.hokudai.ac.jp (KS); smaeda@eis.hokudai.ac.jp (SM).

Abstract

Analysis of reaction on a solid surface is important task for understanding catalytic reaction mechanism. In this study, we studied CO oxidation on Pt(111) surface by using the artificial force induced reaction (AFIR) method. Systematic reaction path search was done, and the reaction route network was created. This network included not only bond rearrangement paths but also migration paths of adsorbed species. Then, the obtained network was analyzed using a kinetics method called rate constant matrix contraction (RCMC). It is found that the bottleneck of the overall reaction is CO₂ generation step from an adsorbed CO molecule and O atom. This result is consistent with the Langmuir-Hinshelwood (LH) mechanism with O₂ dissociation discussed in previous studies. The present procedure, i.e., construction of the reaction route network by the AFIR method followed by an application of the RCMC kinetics method to the resultant reaction route network, was fully systematic and uncovered two aspects: impact of existence of multiple paths in each bond rearrangement step and entropic contribution arisen from short-range migration of adsorbed species.

Introduction

Heterogeneous catalysts have widely been used industrially. They are preferred because of their robustness and lower operating cost, particularly easier separation from the products, than homogeneous catalysts. One of the major applications of the heterogeneous catalysts is an automotive catalytic converter in which oxidation of carbon monoxide to carbon dioxide, $2\text{CO} + \text{O}_2 \rightarrow 2\text{CO}_2$, proceeds with the help of the surface of finely divided metal particles from the platinum group such as platinum (Pt), palladium (Pd), and rhodium (Rh).^{1,2} Thus, the oxidation of CO on Pt(111) surface has been well studied as a model system of heterogeneous catalytic reactions.²⁻²³ This reaction is relatively simple and does not involve reconstructions of the Pt(111) surface.²⁴ Nevertheless, the overall reaction mechanism on the surface could be complicated because it includes not only bond rearrangement (dissociation and association) processes between CO and O₂, but also adsorption (chemisorption), desorption, and surface diffusion (migration) processes. It is known that an O₂ molecule prefers the dissociative adsorption on Pt(111) surface rather than molecular adsorption except at low temperature.^{17,25-28} The CO₂ generation path from adsorbed CO molecule and dissociated O atom has been investigated on various surfaces as well as on Pt(111) surface.^{2-16,18,19,21,22,29-31} Also, the CO₂ production pathway via the OC-OO complex formation has been reported especially on the CO-poisoned surface^{18,23} and on metal nanoparticles.³¹

In most previous theoretical studies of surface reaction analysis using density functional theory (DFT) calculations, the reaction paths that are assumed to be important were calculated by using geometry optimization method, such as the nudged elastic band (NEB) method.^{9-11,13,14,17,31,32} Alternatively, *ab initio* molecular dynamics (AIMD) simulations of surface reactions were also performed,^{33,34} however, it is difficult to complete the whole reaction by AIMD simulations because of the limit of timescale (the reaction should include many elementary steps that occur in a variety of timescales ranging from 10⁻¹⁵

to 10^3 s). To effectively sample slow reaction processes, rare-event simulation techniques such as meta-dynamics simulations^{35,36} and the blue moon ensemble (BME) method^{29,37} are widely used. If the list of elementary steps is provided, time evolution of the system can be simulated by the kinetic Monte Carlo (kMC) method.³⁸ In addition to these methods, the heuristic method which creates connective patterns of molecules and estimates potential energies by machine learning was proposed.³⁹ These methods are still difficult to perform a comprehensive analysis because it is not obvious that which reaction coordinate should be selected or how bias should be considered.

In recent years, the methods which can perform a systematic and automatic path search have been developed by ourselves⁴⁰⁻⁵⁰ and the other groups.⁵¹⁻⁶³ They could be promising to construct the entire path network without any biases. Some of these methods have been applied to surface reactions.⁶⁴⁻⁶⁸ Our artificial force induced reaction (AFIR) method has also been extended to perform global reaction route mapping for surface adsorbed molecules and applied to H₂O on Cu(111) surface, where the resultant global reaction route network was systematically analyzed by the rate constant matrix contraction (RCMC) method.⁶⁸ In this study, our surface reaction analysis method using the whole reaction route network has been applied to CO oxidation on Pt(111) surface. From systematic reaction path search, complex reaction route network including both bond rearrangement paths and short-range migration paths was obtained. Furthermore, kinetics analyses including two kinds of CO₂ generation paths, an entropic contribution of short-range migration paths, and the lifetime of minor species were done using the reaction route network, considering temperature dependency.

Computational method

DFT calculation

The density functional theory (DFT) calculation with the Perdew–Burke–Ernzerhof (PBE) functional and the DZP basis set implemented in SIESTA 4.0 program^{69,70} was used for calculating the potential energy and its gradient. The pseudopotentials were prepared using the parameters in the GGA pseudopotential database;⁷¹ the relativistic pseudopotential which includes the nonlinear core correction (NLCC) was applied to a platinum atom, but the nonrelativistic pseudopotential without NLCC was applied to a carbon or an oxygen atom. The smearing parameter of 10 000 K was chosen for the Methfessel–Paxton scheme.⁷² The Monkhorst–Pack grid, which decides k -point sampling, and the mesh cutoff were changed depending on the calculation as described below.

Preparation of a Pt(111) surface

A periodic slab model was used to compute the chemical reactions on a Pt(111) surface throughout this study. First, the lattice parameter of the face centered cubic (fcc) primitive cell of Pt was optimized at the PBE/DZP level of theory. In this step, an $8 \times 8 \times 8$ Monkhorst–Pack grid was used to sample the Brillouin zone. The mesh cutoff was set to 200.0 Ry. The optimized lattice constant of the fcc lattice was 4.0319 Å, which was slightly longer than experimental one (3.9242 Å).⁷³ Then, the Pt(111) surface was obtained by cutting the optimized fcc crystal of Pt. Finally, a periodic slab model was composed of two layers of the Pt(111) surface (16 atoms per layer) and a vacuum region of 15 Å. In the subsequent calculations, all the translation vectors of the unit cell and Pt atoms were fixed to the initial positions. We confirmed this frozen two-layered slab model is reasonable and free from the effect of the number of surface layers or adsorption-induced surface relaxations (See

Supplementary Information Section S1).

Making a global reaction route network of CO + O₂ on the Pt(111) surface

The strategy to make a global reaction route network of a CO and an O₂ molecules co-adsorbed on the Pt(111) surface is the same as our previous report focused on a water molecule adsorbed on the Cu(111) surface.⁶⁸ The artificial force induced reaction (AFIR) method^{50,74} was adopted here. A systematic reaction path search by using the single-component (SC-) AFIR method⁷⁴ was started from the initial structure shown in Fig. 1. The idea of the AFIR method is to induce reaction by adding artificial forces between two “fragments” (the fragment to be defined automatically and systematically from the atoms in the system); the model collision energy parameter $\gamma = 250 \text{ kJ mol}^{-1}$ in the AFIR function was adopted in the search. The central Pt dimer and atoms in CO and O₂ were considered as “target atoms” in the SC-AFIR algorithm. To prevent getting structures of the same translational symmetry, additional weak biases were also applied between the central Pt dimer and each atom in the CO and O₂ with the parameter $\gamma = 25 \text{ kJ mol}^{-1}$. In this SC-AFIR search, the mesh cutoff and the Monkhorst–Pack grid for the DFT calculation were set to 150 Ry and $1 \times 1 \times 1$, respectively.

Using the locally updated planes (LUP) method,^{75,76} the obtained AFIR paths were re-optimized without the biases to the LUP paths. The LUP method optimizes discrete path points toward the direction perpendicular to path tangent. An obtained LUP path is good approximation of the corresponding intrinsic reaction coordinate (IRC) path.^{77,78} The normal mode analyses were performed at all local minima (MINs) and path top (PT) points of the LUP paths. As described below, the PT points on LUP paths acting as a bottleneck of overall reactions were further optimized to actual transition states (TSs). The mesh cutoff and the Monkhorst–Pack grid for the DFT calculation were set to 150 Ry and $2 \times 2 \times 1$, respectively.

The LUP path network gives qualitative overview of reaction mechanism. For more quantitative reaction kinetics analysis, further LUP calculations were done for the bottleneck paths. To select such paths, the rate constant matrix contraction (RCMC) method^{79,80} was applied. In this method, a $p \times p$ rate constant matrix that includes p MINs of the path network contracts recursively to a $q \times q$ rate constant matrix that represents transitions between q superstates, where each superstate is expressed as a weighted sum of all original states (MINs on the path network). The RCMC method gives a few superstates that interconvert with each other at longer than a certain timescale t , and each superstate includes MINs that can interconvert within t . Each element of the original $p \times p$ rate constant matrix, it being the same as the elementary step from state X to state Y via a TS (or PT), was calculated by the following equation based on canonical transition state theory:⁷⁹

$$k_{X \rightarrow Y} = \Gamma \frac{k_B T}{h} e^{-(\Delta G_{TS} - \Delta G_X)/RT} \quad (1)$$

ΔG_X and ΔG_{TS} are the relative Gibbs free energy values for X and TS (or PT), respectively. k_B is the Boltzmann constant, T is the temperature, h is the Planck constant, and R is the gas constant.

$$\Gamma = 1 + \frac{1}{24} \left(\frac{h\nu^\ddagger}{k_B T} \right)^2 \quad (2)$$

is called the Wigner correction, which has been widely used as a one-dimensional tunneling correction. ν^\ddagger is the magnitude of the imaginary frequency at the TS (or PT).

From the reaction route network, the path which behaves as bottleneck can be extracted as follows. First, RCMC is applied to obtain a contracted network consisting of q superstates, and we consider ω_{iX} , which stands for a contribution from original state X to superstate i ,

$$\sum_{i=1}^q \omega_{iX} = 1 \quad (3)$$

Then, the path is regarded as the bottleneck between different superstates i and j , that is connecting original states X and Y , and fills following three conditions simultaneously.

$$\omega_{iX}\omega_{jY} > 0.25 \quad (4) \quad ,$$

$$\omega_{iX}\omega_{jY} > \omega_{iX}\omega_{iY} \quad (5) \quad ,$$

$$\omega_{iX}\omega_{jY} > \omega_{jX}\omega_{jY} \quad (6) \quad .$$

In this study, $t = 1.0 \times 10^{-1}$ s was adopted to the timescale and three different temperatures, $T = 300, 500, 1000$ K, were used. By RCMC, the highest energy points along the path were selected as the bottleneck, and LUP path refinement calculations were performed; a LUP calculation of a selected path continued unless the PT of the selected path converged to an accurate TS. Use of such a PT/TS hybrid network was introduced and justified for discussions on reaction steps taking longer timescales than t ($= 1.0 \times 10^{-1}$ s in this study) in our previous study.⁶⁸

Results and Discussion

Reaction route network

By our systematic search for the reaction route network of the CO oxidation on Pt(111) surface, 139 MINs and 572 LUP paths (including 545 PTs and 27 TSs) were found. Fig. 2 depicts the obtained reaction route network which consists of 133 nodes (MINs) and 298 edges (LUP paths) including 26 TSs. 6 of 139 MINs were truncated because they became a non-connected network due to numerical problems occurring in the LUP calculation process. It can happen when numerical parameters such as the Monkhorst–Pack grid are changed depending on the search and LUP path refinement stages, but this was not a serious problem because most parts in the entire network did not change significantly. The LUP paths returning back to the same MIN are not shown on the network for simplicity. Only the lowest LUP path is represented when there are two or more paths connecting the same MIN pair. A bottleneck path is drawn by thick line and a thin line corresponds to a non-bottleneck path.

There are six different adsorption states in this reaction route network: $\text{CO} + \text{O}_2$, $\text{CO} + 2\text{O}$, $\text{CO}_2 + \text{O}$, $\text{CO}_2(\text{g}) + \text{O}$, OC-OO , and CO_3 , where CO_2 and $\text{CO}_2(\text{g})$ stand for a bent CO_2 molecule chemisorbed on the Pt(111) surface and a linear CO_2 weakly bound to the Pt(111) surface, respectively. CO molecule, O_2 molecule, O atom and other obtained species were chemisorbed on Pt(111) surface. The most stable structure of each adsorption state is shown in Fig. 3. Energy values of the structures in Fig. 3 are represented as the relative Gibbs free energy value to the total energy of $\text{CO}(\text{g})$, $\text{O}_2(\text{g})$, and Pt(111) surface. Although this is a simple system that only four atoms react on the surface, the obtained reaction route network is complicated. This is because the network includes both bond rearrangement paths and migration paths.

Stability of stable structure depends on adsorption state of each adsorbed species and its relative position. The most stable structure in the reactant state is MIN114, and it is shown in Figure 3(a). In MIN114, the CO molecule is adsorbed in the fcc hollow site and the O₂ molecule is adsorbed in bridge (t-b-t) state. We note that the most stable adsorption state of CO molecule in this calculation is inconsistent with experimental results that suggest the most favorable adsorption site of CO molecule is atop site.⁸¹⁻⁸⁵ This problem is known as CO puzzle, and we discuss the adsorption sites and energies in Supplementary Information (See Section S2).

Mechanism from reaction route network

We have developed the RCMC method which helps extracting reaction mechanisms from a complicated reaction route network.^{79,80} The RCMC method provides a $q \times q$ rate constant matrix that represents transitions between q superstates by recursively contracting an original $p \times p$ rate constant matrix ($p = 133$ in this case), where, in each superstate, local equilibrium among MINs contributing to the superstate is assumed. Fig. 4 depicts the superstates at the temperature $T = 300$ K, and in three different timescales, $t = 1.0 \times 10^{-1}$, 1.0, or 1.0×10^3 s. Although the case of $t = 1.0 \times 10^1$ and 1.0×10^2 s was also analyzed, the result is same as $t = 1.0$ s. Similar hierarchical analysis in terms of timescale was also performed previously for an organic reaction.⁸⁶ In Fig. 4, the numerical values indicate the reaction barriers between the superstates. They were calculated from logarithm of overall rate constant, given as off-diagonal terms of $q \times q$ rate constant matrix obtained from the result of the RCMC applied to the original 133×133 rate constant matrix, where $q = 3, 2,$ and 1, respectively, in the RCMC results with $t = 1.0 \times 10^{-1}, 1.0,$ or 1.0×10^3 s.

First, when timescale is set to $t = 1.0 \times 10^{-1}$ s as shown in Fig. 4(a), the network is contracted into three superstates, SS0, SS1, and SS2. The representative structure in each

superstate is $\text{CO} + \text{O}_2$ (SS0), $\text{CO} + 2\text{O}$ (SS1), and $\text{CO}_2(\text{g}) + \text{O}$ (SS2), respectively. SS2 also includes three other adsorption states, CO_3 , OC-OO , and $\text{CO}_2 + \text{O}$, because these states decay quickly into $\text{CO}_2(\text{g}) + \text{O}$ in a shorter timescale than 1.0×10^{-1} s, where lifetimes of these minor states are about 10^{-12} , 10^{-9} , and 10^{-4} s, respectively.

Overall rate constants of k_1 and k_2 of Fig. 4(a) were compared as shown in Table 1, where k_1 and k_2 corresponds to an O_2 dissociation process and a direct CO_2 generation process through OC-OO type MIN or TS, respectively. From Table 1, it was found that the contribution of the minor path is $\sim 10\%$ in all temperature ranges considered. This implies that CO_2 formation via O_2 dissociation is more favorable.

Next, if timescale was extended to $t = 1.0$ s, the reaction path network can be contracted to two superstates. The two superstates, SS0 and SS1 at $t = 1.0 \times 10^{-1}$ s, are contracted to one superstate at $t = 1.0$ s depicted in Fig. 4(b). Hence, at $t = 1.0$ s, paths connecting a MIN in SS0 and the other MIN in SS1 can be regarded as the bottleneck in the entire network. From this result, the bottleneck step of the CO oxidation on the $\text{Pt}(111)$ surface is formation of CO_2 from adsorbed CO molecule and O atom. The result is consistent with previous studies which concluded that the reaction proceeds along the LH mechanism.

Finally, all original states are contracted to one superstate at $t = 1.0 \times 10^3$ s as shown in Fig. 4(c). This means all of the reaction can occur within this timescale. By applying the RCMC method with different t , the timescale hierarchy of the present reaction was elucidated.

As mentioned above, two different CO_2 generation paths are known from previous studies. Energy profiles at $T = 300$ K for the two CO_2 formation channels extracted from the network are shown in Fig. 5. This energy profile is a simplified model consisting of the energy of the most stable structure of each adsorption state and the connecting path whose TS / PT has the lowest energy. We call this simplified model as the lowest conformer to single

transition state (LC-TS) model.⁷⁹ According to Fig. 5, the rate-determining step is the second step that corresponds to the $\text{CO} + 2\text{O} \rightarrow \text{CO}_2(\text{g}) + \text{O}$ process in the case of (i) *via* O_2 dissociation, whereas it is the first step in which $\text{CO} + \text{O}_2 \rightarrow \text{OC-OO}$ proceeds in the case of (ii) *via* the OC-OO complex. The final step ($\text{CO}_2 + \text{O} \rightarrow \text{CO}_2(\text{g}) + \text{O}$) is not depicted in Fig. 5 for simplicity, because the barrier of this step is very small, about 2.3 kJ mol^{-1} . The reaction barrier of the LC-TS model can be compared to other theoretical studies. In the case of (i) *via* O_2 dissociation route, the reaction barrier of the first step ($\text{CO} + \text{O}_2 \rightarrow \text{CO} + 2\text{O}$) is 69.7 kJ mol^{-1} (73.5 kJ mol^{-1} in electronic energy), and that of the second step ($\text{CO} + 2\text{O} \rightarrow \text{CO}_2(\text{g}) + \text{O}$) is 89.2 kJ mol^{-1} (90.5 kJ mol^{-1} in electronic energy). This indicates our result is in the range of previous theoretical studies, $27.0\text{--}74.3 \text{ kJ mol}^{-1}$ (in Refs. 14 and 17) and $37.6\text{--}111.9 \text{ kJ mol}^{-1}$ (in Refs. 9–12,14–16, and 29), respectively. Although (ii) the route *via* OC-OO complex on the clean Pt(111) surface has not been calculated to our knowledge, but similar route was suggested from both experimental and theoretical studies.^{18,23}

Impact of reaction route network

To see impact of the reaction route network on the overall kinetics, the result of RCMC was compared with that of simplified models. The rate constants obtained by the RCMC method include entropic contributions arisen from transitions among many structures which have same adsorption states but different relative positions, and many reaction paths connected to these structures. Therefore, the rate constant value obtained by the RCMC method is different from that by the LC-TS model. The difference is called conformational entropy.⁷⁹ There are two types of conformational entropy. One is conformational entropy of MINs arising from a variety of MINs and this contributes to decrease the rate constant. The other is

conformational entropy of TSs arisen from various configuration at bond rearrangement TS and contributes to increase the rate constant.

How much the conformational entropy of MINs and TSs affects the overall rate constants can be discussed by comparing rate constants obtained by the RCMC method with those excluding these entropic contributions. Therefore, in addition to k_1 , k_2 , and k_3 by RCMC denoted as $k_x(\text{RCMC})$, those by LC-TS denoted as $k_x(\text{LC-TS})$ and by a lowest conformer to multiple transition states (LC-mTS) model denoted as $k_x(\text{LC-mTS})$, were computed. In computation of $k_x(\text{LC-TS})$, the free energy gap $\Delta\Delta G$ between the lowest conformer in the reactant region and the lowest bottleneck TS to the product region was substituted to the rate constant expression of the transition state theory. While, $k_x(\text{LC-mTS})$ was computed as the sum of rate constants computed by substituting the free energy gap $\Delta\Delta G$ between the lowest conformer in the reactant region and a bottleneck TS to the product region to the rate constant expression of the transition state theory, where the sum is take over all bottleneck TSs to the product region. The difference between $k_x(\text{LC-TS})$ and $k_x(\text{LC-mTS})$ corresponds to contribution of conformational entropy of TSs, whereas the difference between $k_x(\text{LC-mTS})$ and $k_x(\text{RCMC})$ corresponds to contribution of conformational entropy of MINs.

Table 2 shows k_1 , k_2 , and k_3 at $T = 300, 500, 1000$ K, computed by the three different models, RCMC, LC-TS, and LC-mTS. In order to visualize the differences clearly, ratios of $k_x(\text{LC-TS})$ and $k_x(\text{LC-mTS})$ with reference to $k_x(\text{RCMC})$ are depicted in Fig. 6. In Fig. 6, the ratios do not vary monotonically depending on T because the lowest conformer as well as the lowest bottleneck TS changes depending on T . However, we can see some trends in the Fig.. First, the conformational entropy of TSs affected all the k_x ($x = 1-3$) values, making $k_x(\text{LC-mTS})$ 2~3 times of $k_x(\text{LC-TS})$. This indicates significance of existence of multiple TSs with different configurations in each chemical bond rearrangement process. Its importance has also been discussed in studies on chemical selectivity and reactivity of various chemical

reactions.⁸⁸⁻⁹⁶ Fig. 6 clearly show that the conformational entropy of TS has certain impact on the CO oxidation on Pt(111) surface.

Second, the conformational entropy of MINs is small in k_3 especially at low temperature, according to the deviation of $k_x(\text{LC-mTS})$ from $k_x(\text{RCMC})$. This is consistent with our chemical knowledge that in SS1 all the chemical species, *i.e.*, two O atoms and a CO molecule, are bound strongly to the Pt(111) surface. This suppressed the surface migration in SS1 and made the conformational entropy of MIN small. On the other hand, k_1 and k_2 showed a relatively large conformational entropy of MINs, because the binding energy of O₂ to the Pt(111) surface is much smaller than that of an O atom and CO.

Overall, the simple LC-TS model showed a reasonable agreement with $k_x(\text{RCMC})$ for k_1 and k_2 because of an error cancelation between the two conformational entropy contributions. Nevertheless, an error cancelation is not expected always. The $k_x(\text{RCMC})$ based on the reaction route network by the AFIR method would thus be promising in evaluating rate constants of elementary steps of surface reactions because it naturally includes conformational entropy of both MINs and TSs.

Concluding remarks

In this study, a systematic reaction path search by using the AFIR method was carried out for the CO oxidation on the Pt(111) surface. Then, the reaction route network consisting of 133 MINs was obtained through the automated exploration. The network included not only bond rearrangement paths but also short-range migration paths. The RCMC kinetics method was applied to the reaction route network to analyze it systematically, and it was revealed that the bottleneck of the entire reaction is the CO₂ generation step involving the recombination between an adsorbed CO molecule and O atom. Furthermore, contributions of two different CO₂ generation paths, via O₂ dissociation and via OC-OO complex formation, were discussed. In addition, the reaction route network included minor species such as CO₂ + O, OC-OO, and CO₃ as short-lived intermediates. It should be emphasized that no prior assumption about the reaction mechanism was made for obtaining the present results.

The present reaction route network includes short-range migration paths explicitly. Its impact on the overall rate constants was discussed in detail comparing rate constants computed by three different models. It was discussed that entropic contributions of MIN and TS arisen from variety of configurations taken at stable and transition states shifted the overall rate constants downward and upward, respectively. The present approach combining AFIR and RCMC would thus be promising to obtain rate constants including entropic contributions of the short-range migration. Connecting our approach with kinetic Monte Carlo simulations taking account of surface coverage and collision frequency of adsorbed species would be an interesting future subject.

Conflicts of interest

There are no conflicts to declare.

Acknowledgements

This work was partly supported by a grant from the Japan Science and Technology Agency for Core Research for Evolutional Science and Technology (CREST) in the Area “Establishment of Molecular Technology toward the Creation of New Functions” (Grant No. JPMJCR14L5) at Hokkaido University. K. Sugiyama and M. Takagi were supported by the Ministry of Education, Culture, Sports, Science and Technology through the Program for Leading Graduate Schools (Hokkaido University “Ambitious Leader’s Program”).

Supplementary material

The molecular geometries of the initial structure of the SC-AFIR search (MIN127 shown in Fig. 1), and the most stable structure of each adsorbed state (MIN0, MIN53, MIN58, MIN83, MIN114, MIN131, shown in Fig. 3) are provided in the CIF (crystallography information file) format. The 26 TS structures are also available in the CIF format.

References

1. J. Kašpar, P. Fornasiero and N. Hickey, Automotive Catalytic Converters: Current Status and Some Perspectives, *Catal. Today*, 2003, **77**, 419–449.
2. G. Ertl, Reactions at Surfaces: From Atoms to Complexity (Nobel Lecture), *Angew. Chem. Int. Ed.*, 2008, **47**, 3524–3535.
3. R. L. Palmer and J. N. Smith, Jr., Molecular Beam Study of CO Oxidation on a (111) Platinum Surface, *J. Chem. Phys.*, 1974, **60**, 1453–1463.
4. C. T. Campbell, G. Ertl, H. Kuipers and J. Segner, A molecular Beam Study of the Catalytic Oxidation of CO on a Pt(111) Surface, *J. Chem. Phys.*, 1980, **73**, 5862–5873.
5. J. L. Gland and E. B. Kollin, Carbon Monoxide Oxidation on the Pt(111) Surface: Temperature Programmed Reaction of Coadsorbed Atomic Oxygen and Carbon Monoxide, *J. Chem. Phys.*, 1983, **78**, 963–974.
6. C. Hardacre, R. M. Ormerod and R. M. Lambert, Low-Temperature Carbon Monoxide Oxidation on Pt(111). Dependence of Apparent Activation Energy on Reactant Gas Composition, *Chem. Phys. Lett.*, 1993, **206**, 171–174.
7. G. Ertl, Reactions at Well-Defined Surfaces, *Surf. Sci.*, 1994, **299–300**, 742–754.
8. J. Wintterlin, S. Volkening, T. V. W. Janssens, T. Zambelli, and G. Ertl, Atomic and Macroscopic Reaction Rates of a Surface-Catalyzed Reaction, *Science*, 1997, **278**, 1931–1934.
9. A. Eichler and J. Hafner, Reaction Channels for the Catalytic Oxidation of CO on Pt(111), *Phys. Rev. B*, 1999, **59**, 5960–5967.
10. R. J. Baxter and P. Hu, Insight into Why the Langmuir-Hinshelwood Mechanism Is Generally Preferred, *J. Chem. Phys.*, 2002, **116**, 4379–4381.
11. A. Eichler, CO Oxidation on Transition Metal Surfaces: Reaction Rates from First Principles, *Surf. Sci.*, 2002, **498**, 314–320.

12. X.-Q. Gong, Z.-P. Liu, R. Raval and P. Hu, A Systematic Study of CO Oxidation on Metals and Metal Oxides: Density Functional Theory Calculations, *J. Am. Chem. Soc.*, 2004, **126**, 8–9.
13. S. Kandoi, A. A. Gokhale, L. C. Grabow, J. A. Dumesic, and M. Mavrikakis, Why Au and Cu Are More Selective than Pt for Preferential Oxidation of CO at Low Temperature, *Catal. Lett.*, 2004, **93**, 93–100.
14. L. Grabow, Y. Xu and M. Mavrikakis, Lattice Strain Effects on CO Oxidation on Pt(111), *Phys. Chem. Chem. Phys.*, 2006, **8**, 3369–3374.
15. M. Nagasaka, H. Kondoh, I. Nakai and T. Ohta, CO Oxidation Reaction on Pt(111) Studied by the Dynamic Monte Carlo Method Including Lateral Interactions of Adsorbates, *J. Chem. Phys.*, 2007, **126**, 044704 (7 pages).
16. H. Falsig, B. Hvoæk, I. S. Kristensen, T. Jiang, T. Bligaard, C. H. Christensen and J. K. Nørskov, Trends in the Catalytic CO Oxidation Activity of Nanoparticles, *Angew. Chem. Int. Ed.*, 2008, **47**, 4835–4839.
17. B. Shan, N. Kapur, J. Hyn, L. Wang, J. B. Nicholas and K. Cho, CO-Coverage-Dependent Oxygen Dissociation on Pt(111) Surface, *J. Phys. Chem. C*, 2009, **113**, 710–715.
18. A. D. Allian, K. Takanabe, K. L. Furdala, X. Hao, T. J. Truex, J. Cai, C. Buda, M. Neurock and E. Iglesia, Chemisorption of CO and Mechanism of CO Oxidation on Supported Platinum Nanoclusters, *J. Am. Chem. Soc.*, 2011, **133**, 4498–4517.
19. A. Farkas, K. Zalewska-Wierzbicka, C. Bachmann, J. Goritzka, D. Langsdorf, O. Balmes, J. Janek and H. Over, High Pressure Carbon Monoxide Oxidation over Platinum (111), *J. Phys. Chem. C*, 2013, **117**, 9932–9942.

20. S. K. Calderón, M. Grabau, L. Óvári, B. Kress, H.-P. Steinrück and C. Papp, CO Oxidation on Pt(111) at Near Ambient Pressures, *J. Chem. Phys.*, 2016, **144**, 044706 (9 pages).
21. M. A. van Spronsen, J. W. M. Frenken and I. M. N. Groot, Surface Science Under Reaction Conditions: CO Oxidation on Pt and Pd Model Catalysts, *Chem. Soc. Rev.*, 2017, **46**, 4347–4374.
22. H. Ueta and M. Kurahashi, Steric Effect in CO Oxidation on Pt(111), *J. Chem. Phys.*, 2017, **147**, 194705 (4 pages).
23. J. Kim, M. C. Noh, W. H. Doh and J. Y. Park, In Situ Observation of Competitive CO and O₂ Adsorption on the Pt(111) Surface Using Nnear-Ambient Pressure Scanning Tunneling Microscopy, *J. Phys. Chem. C*, 2018, **122**, 6246–6254.
24. A. R. Sandy, S. G. J. Mochrie, D. M. Zehner, G. Grübel, K. G. Huang and D. Gibbs, Reconstruction of the Pt(111) Surface, *Phys. Rev. Lett.*, 1992, **68**, 2192–2195.
25. H. Steininger, S. Lehwald and H. Ibach, Adsorption of Oxygen on Pt(111), *Surf. Sci.*, 1982, **123**, 1–17.
26. A. Eichler and J. Hafner, Molecular Precursors in the Dissociative Adsorption of O₂ on Pt(111), *Phys. Rev. Lett.*, 1997, **79**, 4481–4484.
27. A. Groß, A. Eichler, J. Hafner, M. J. Mehl and D. A. Papaconstantopoulos, Unified Picture of the Molecular Adsorption Process: O₂/Pt(111), *Surf. Sci.*, 2003, **539**, L542–L548.
28. A. Eichler, F. Mittendorfer and J. Hafner, Precursor-Mediated Adsorption of Oxygen on the (111) Surfaces of Platinum-Group Metals, *Phys. Rev. B*, 2000, **62**, 4744–4755.
29. K. Koizumi, K. Nobusada and M. Boero, Reducing the Cost and Preserving the Reactivity in Noble-Metal-Based Catalysts: Oxidation of CO by Pt and Al-Pt Alloy Clusters Supported on Graphene, *Chem. Eur. J.*, 2016, **22**, 5181–5188.

30. S. Piccinin and M. Stamatakis, Steady-State CO Oxidation on Pd(111): First-Principles Kinetic Monte Carlo Simulations and Microkinetic Analysis, *Top Catal*, 2017, **60**, 141–151.
31. N. Lopez and J. K. Nørskov, Catalytic CO Oxidation by a Gold Nanoparticles: A Density Functional Theory, *J. Am. Chem. Soc.*, 2002, **124**, 11262–11263.
32. P.-T. Chen, E. C. Tyo, M. Hayashi, M. J. Pellin, O. Safonova, M. Nachtegaal, J. A. Bokhoven, S. Vajda and P. Zapol, Size-Selective Reactivity of Subnanometer Ag₄ and Ag₁₆ Clusters on a TiO₂ Surface, *J. Phys. Chem. C*, 2017, **121**, 6614–6625.
33. L. Agosta, E. G. Brandt and A. P. Lyubartsev, Diffusion and Reaction Pathways of Water Near Fully Hydrated TiO₂ Surfaces from *Ab Initio* Molecular Dynamics, *J. Chem. Phys.*, 2017, **147**, 024704 (16 pages).
34. L. Zhou, X. Zhou, M. Alducin, L. Zhang, B. Jiang and H. Guo, *Ab Initio* Molecular Dynamics Study of the Eley-Rideal Reaction of H + Cl-Au(111) → HCl + Au(111): Impact of Energy Dissipation to Surface Phonons and Electron-Hole Pairs, *J. Chem. Phys.*, 2018, **148**, 014702 (8 pages).
35. T. Cheng, H. Xiao and W. A. Goddard, III, Free-Energy Barriers and Reaction Mechanisms for the Electrochemical Reduction of CO on the Cu(100) Surface, Including Multiple Layers of Explicit Solvent at pH 0, *J. Phys. Chem. Lett.*, 2015, **6**, 4767–4773.
36. T. Cheng, W. A. Goddard, III, Q. An, H. Xiao, B. Merinov and S. Morozov, Mechanism and Kinetics of the Electrocatalytic Reaction Responsible for the High Cost of Hydrogen Fuel Cells, *Phys. Chem. Chem. Phys.*, 2017, **19**, 2666–2673.
37. A. Tilocca and A. Selloni, Reaction Pathway and Free Energy Barrier for Defect-Induced Water Dissociation on the (101) Surface of TiO₂-Anatase, *J. Chem. Phys.*, 2003, **119**, 7445–7450.

38. D.-J. Liu, A. Garcia, J. Wang, D. M. Ackerman, C.-J. Wang and J. W. Evans, Kinetic Monte Carlo Simulation of Statistical Mechanical Models and Coarse-Grained Mesoscale Descriptions of Catalytic Reaction–Diffusion Processes: 1D Nanoporous and 2D Surface Systems, *Chem. Rev.*, 2015, **115**, 5979–6050.
39. C. F. Goldsmith and R. H. West, Automatic Generation of Microkinetic Mechanisms for Heterogeneous Catalysis, *J. Phys. Chem. C*, 2017, **121**, 9970–9981.
40. K. Ohno and S. Maeda, A Scaled Hypersphere Search Method for the Topography of Reaction Pathways on the Potential Energy Surface, *Chem. Phys. Lett.*, 2004, **384**, 277–282.
41. S. Maeda and K. Ohno, Global Mapping of Equilibrium and Transition Structures on Potential Energy, *J. Phys. Chem. A*, 2005, **109**, 5742–5753.
42. K. Ohno and S. Maeda, Global Reaction Route Mapping on Potential Energy Surfaces of Formaldehyde, Formic Acid, and Their Metal-Substituted Analogues, *J. Phys. Chem. A*, 2006, **110**, 8933–8941.
43. K. Ohno and S. Maeda, Automated Exploration of Reaction Channels, *Phys. Scr.*, 2008, **78**, 058122 (8 pages).
44. S. Maeda and K. Morokuma, Communications: A Systematic Method for Locating Transition Structures of $A + B \rightarrow X$ Type Reactions, *J. Chem. Phys.*, 2010, **132**, 241102 (4 pages).
45. S. Maeda and K. Morokuma, Finding Reaction Pathways of Type $A + B \rightarrow X$: Toward Systematic Prediction of Reaction Mechanisms, *J. Chem. Theory Comput.*, 2011, **7**, 2335–2345.
46. S. Maeda, K. Ohno and K. Morokuma, Systematic Exploration of the Mechanism of Chemical Reactions: The Global Reaction Route Mapping (GRRM) Strategy Using the ADDF and AFIR Methods, *Phys. Chem. Chem. Phys.*, 2013, **15**, 3683–3701.

47. S. Maeda, T. Taketsugu and K. Morokuma, Exploring Transition State Structures for Intramolecular Pathways by the Artificial Force Induced Reaction Method, *J. Comput. Chem.*, 2014, **35**, 166–173.
48. S. Maeda, T. Taketsugu, K. Morokuma and K. Ohno, Anharmonic Downward Distortion Following for Automated Exploration of Quantum Chemical Potential Energy Surfaces, *Bull. Chem. Soc. Jpn.*, 2014, **87**, 1315–1334.
49. W. M. C. Sameera, S. Maeda and K. Morokuma, Computational Catalysis Using the Artificial Force Induced Reaction Method, *Acc. Chem. Res.*, 2016, **49**, 763–773.
50. S. Maeda, Y. Harabuchi, M. Takagi, T. Taketsugu and K. Morokuma, Artificial Force Induced Reaction (AFIR) Method for Exploring Quantum Chemical Potential Energy Surfaces, *Chem. Rec.*, 2016, **16**, 2232–2248.
51. D. J. Wales, J. P. K. Doye, M. A. Miller, P. N. Mortenson and T. R. Walsh, Energy Landscapes: From Clusters to Biomolecules, *Adv. Chem. Phys.*, 2000, **115**, 1–111.
52. M. Dallos, H. Lischka, E. V. D. Monte, M. Hirsch and W. Quapp, Determination of Energy Minima and Saddle Points Using Multireference Configuration Interaction Methods in Combination with Reduced Gradient Following: The S_0 Surface of H_2CO and the T_1 and T_2 Surfaces of Acetylene, *J. Comput. Chem.*, 2002, **23**, 576–583.
53. J. Baker and K. Wolinski, Isomerization of Stilbene Using Enforced Geometry Optimization, *J. Comput. Chem.*, 2011, **32**, 43–53.
54. P. M. Zimmerman, Automated Discovery of Chemically Reasonable Elementary Reaction Steps, *J. Comput. Chem.*, 2013, **34**, 1385–1392.
55. D. Rappoport, C. J. Galvin, D. Y. Zubarev and A. Aspuru-Guzik, Complex Chemical Reaction Networks from Heuristics-Aided Quantum Chemistry, *J. Chem. Theory Comput.*, 2014, **10**, 897–907.

56. B. Schaefer, S. Mohr, M. Amsler and S. Goedecker, Minima Hopping Guided Path Search: An Efficient Method for Finding Complex Chemical Reaction Pathways, *J. Chem. Phys.*, 2014, **140**, 214102 (13 pages).
57. D. J. Wales, Perspective: Insight into Reaction Coordinates and Dynamics from the Potential Energy Landscape, *J. Chem. Phys.*, 2015, **142**, 130901 (12 pages).
58. S. Habershon, Sampling Reactive Pathways with Random Walks in Chemical Space: Applications to Molecular Dissociation and Catalysis, *J. Chem. Phys.*, 2015, **143**, 094106 (14 pages).
59. E. Martínez-Núñez, An Automated Method to Find Transition States Using Chemical Dynamics Simulations, *J. Comput. Chem.*, 2015, **36**, 222–234.
60. M. Bergeler, G. N. Simm, J. Proppe and M. Reuher, Heuristics-Guided Exploration of Reaction Mechanisms, *J. Chem. Theory Comput.*, 2015, **11**, 5712–5722.
61. X.-J. Zhang and Z.-P. Liu, Reaction Sampling and Reactivity Prediction Using the Stochastic Surface Walking Method, *Phys. Chem. Chem. Phys.*, 2015, **17**, 2757–2769.
62. L.-P. Wang, R. T. McGibbon, V. S. Pande and T. J. Martinez, Automated Discovery and Refinement of Reactive Molecular Dynamics Pathways, *Chem. Theory Comput.*, 2016, **12**, 638–649.
63. M. Yang, J. Zou, G. Wang and S. Li, Automatic Reaction Pathway Search via Combined Molecular Dynamics and Coordinate Driving Method, *J. Phys. Chem. A*, 2017, **121**, 1351–1361.
64. S. Ohno, K. Shudo, M. Tanaka, S. Maeda and K. Ohno, Theoretical Investigation of the Reaction Pathway of O Atom on Si(001)-(2×1), *J. Phys. Chem. C*, 2010, **114**, 15671–15677.

65. X.-J. Zhang, C. Shang and Z.-P. Liu, Stochastic Surface Walking Reaction Sampling for Resolving Heterogeneous Catalytic Reaction Network: A Revisit to the Mechanism of Water-Gas Shift Reaction on Cu, *J. Chem. Phys.*, 2017, **147**, 152706 (9 pages).
66. Z. W. Ulissi, A. J. Medford, T. Bligaard and J. K. Nørskov, To Address Surface Reaction Network Complexity Using Scaling Relations Machine Learning and DFT Calculations, *Nat. Commun.*, 2017, **8**, 14621 (7 pages).
67. S.-D. Huang, C. Shang, X.-J. Zhang and Z.-P. Liu, Material Discovery by Combining Stochastic Surface Walking Global Optimization with a Neural Network, *Chem. Sci.*, 2017, **8**, 6327–6337.
68. S. Maeda, K. Sugiyama, Y. Sumiya, M. Takagi and K. Saita, Global Reaction Route Mapping for Surface Adsorbed Molecules: A Case Study for H₂O on Cu(111) Surface, *Chem. Lett.*, 2018, **47**, 396–399.
69. J. M. Soler, E. Artacho, J. D. Gale, A. García, J. Junquera, P. Ordejón and D. Sánchez-Portal, The SIESTA Method for *Ab Initio* Order-*N* Materials Simulation, *J. Phys.: Condens. Matter*, 2002, **14**, 2745–2779.
70. E. Artacho, J. M. Cella, J. D. Gale, A. García, J. Junquera, R. M. Martin, P. Ordejón, D. Sánchez-Portal and J. M. Soler, *SIESTA 4.0 (Revision 530)*, The Siesta Group, 2016, see <http://www.uam.es/siesta>
71. Translation of Abinit's GGA Pseudo Database to Siesta Format: <https://departments.icmab.es/leem/siesta/Databases/Pseudopotentials/periodictable-gga-abinit.html>
72. M. Methfessel and A. T. Paxton, High-Precision Sampling for Brillouin-Zone Integration in Metals, *Phys. Rev. B*, 1989, **40**, 3616–3621.

73. Y. Waseda, K. Hirata and M. Ohtani, High-Temperature Thermal Expansion of Platinum, Tantalum, Molybdenum, and Tungsten Measured by X-Ray Diffraction, *High Temp. High Press.*, 1975, **7**, 221–226.
74. S. Maeda, Y. Harabuchi, M. Takagi, K. Saita, K. Suzuki, T. Ichino, Y. Sumiya, K. Sugiyama and Y. Ono, Implementation and Performance of the Artificial Force Induced Reaction Method in the GRRM17 Program, *J. Comput. Chem.*, 2018, **39**, 233–250.
75. C. Choi and R. Elber, Reaction Path Study of Helix Formation in Tetrapeptides: Effect of Side Chains, *J. Chem. Phys.*, 1991, **94**, 751–760.
76. P. Y. Ayala and H. B. Schlegel, A Combined Method for Determining Reaction Paths, Minima, and Transition State Geometries, *J. Chem. Phys.*, 1997, **107**, 375–384.
77. K. Fukui, The Path of Chemical Reactions - The IRC Approach, *Acc. Chem. Res.*, 1981, **14**, 363–367.
78. S. Maeda, Y. Harabuchi, Y. Ono, T. Taketsugu and K. Morokuma, Intrinsic Reaction Coordinate: Calculation, Bifurcation, and Automated Search, *Int. J. Quant. Chem.*, 2015, **115**, 258–269.
79. Y. Sumiya, Y. Nagahata, T. Komatsuzaki, T. Taketsugu and S. Maeda, Kinetic Analysis for the Multistep Profiles of Organic Reactions: Significance of the Conformational Entropy on the Rate Constants of the Claisen Rearrangement, *J. Phys. Chem. A*, 2015, **119**, 11641–11649.
80. Y. Sumiya, T. Taketsugu and S. Maeda, Full Rate Constant Matrix Contraction Method for Obtaining Branching Ratio of Unimolecular Decomposition, *J. Comput. Chem.*, 2017, **38**, 101–109.
81. H. Froitzheim, H. Hopster, H. Ibach and S. Lehwald, Adsorption Sites of CO on Pt(111), *Appl. Phys.*, 1977, **13**, 147–151.

82. G. Ertl, M. Newmann and K. M. Streit, Chemisorption of CO on the Pt(111) Surface, *Surf. Sci.*, 1977, **64**, 393–410.
83. P. J. Feibelman, B. Hammer, J. K. Nørskov, F. Wagner, M. Scheffler, R. Stumpf, R. Watwe and J. Dumesic, The CO/Pt(111) Puzzle, *J. Phys. Chem. B*, 2001, **105**, 4018–4025.
84. Y. Wang, S. de Gironcoli, N. S. Hush and J. R. Reimers, Successful a Priori Modeling of CO Adsorption on Pt(111) Using Periodic Hybrid Density Functional Theory, *J. Am. Chem. Soc.*, 2007, **129**, 10402–10407.
85. P. Janthon, F. Viñes, J. Sirijaraensre, J. Limtrakl and F. Illas, Adding Pieces to the CO/Pt(111) Puzzle: The Role of Dispersion, *J. Phys. Chem. C*, 2017, **121**, 3970–3977.
86. Y. Nagahata, S. Maeda, H. Teramoto, T. Horiyama, T. Taketsugu and T. Komatsuzaki, Deciphering Time Scale Hierarchy in Reaction Networks, *J. Phys. Chem. B*, 2016, **120**, 1961–1971.
87. *Cytoscape (Version 3.5.1)*, The Cytoscape Consortium, 2017, see <http://www.cytoscape.org/>
88. S. Maeda and K. Ohno, Lowest Transition State for the Chirality-determining Step in Ru((R)-BINAP)-catalyzed Asymmetric Hydrogenation of Methyl-3-oxobutanoate, *J. Am. Chem. Soc.*, 2008, **130**, 17228–17229
89. P. J. Donoghue, P. Helquist, P. O. Norrby and O. Wiest, Prediction of Enantioselectivity in Rhodium Catalyzed Hydrogenations, *J. Am. Chem. Soc.*, 2009, **131**, 410–411.
90. P. Seal, E. Papajak and D. G. Truhlar, Kinetics of the Hydrogen Abstraction from Carbon-3 of 1-Butanol by Hydroperoxyl Radical: Multi-Structural Variational Transition-State Calculations of a Reaction with 262 Conformations of the Transition State, *J. Phys. Chem. Lett.*, 2012, **3**, 264–271.

91. M. Hatanaka, S. Maeda and K. Morokuma, Sampling of Transition States for Predicting Diastereoselectivity Using Automated Search Method-Aqueous Lanthanide-Catalyzed Mukaiyama Aldol Reaction, *J. Chem. Theory. Comput.*, 2013, **9**, 2882–2886.
92. E. Lime, M. D. Lundholm, A. Forbes, O. Wiest, P. Helquist and P. O. Norrby, Stereoselectivity in Asymmetric Catalysis: The Case of Ruthenium-Catalyzed Ketone Hydrogenation, *J. Chem. Theory. Comput.*, 2014, **10**, 2427–2435.
93. M. Gao, A. Lyalin, S. Maeda and T. Taketsugu, Application of Automated Reaction Path Search Methods to a Systematic Search of Single-Bond Activation Pathways Catalyzed by Small Metal Clusters: A Case Study on H-H Activation by Gold, *J. Chem. Theory Comput.*, 2014, **10**, 1623–1630.
94. M. Gao, A. Lyalin, M. Takagi, S. Maeda and T. Taketsugu, Reactivity of Gold Clusters in the Regime of Structural Fluxionality, *J. Phys. Chem. C*, 2015, **119**, 11120–11130.
95. E. T. Baxter, M.-A. Ha, A. C. Cass, A. N. Alexandrova and S. L. Anderson, Ethylene Dehydrogenation on Pt_{4,7,8} Clusters on Al₂O₃: Strong Cluster Size Dependence Linked to Preferred Catalyst Morphologies, *ACS Catal.*, 2017, **7**, 3322–3335.
96. G. Sun and P. Sautet, Metastable Structures in Cluster Catalysis from First-Principles: Structural Ensemble in Reaction Conditions and Metastability Triggered Reactivity, *J. Am. Chem. Soc.*, 2018, **140**, 2812–2820.

Table 1. Overall rate constants from SS0 to SS1, k_1 , and from SS0 to SS2, k_2 , and contribution of the minor path $k_2 / (k_1 + k_2)$.

T [K]	300	500	1000
k_1 [s^{-1}]	4.39×10^0	5.37×10^5	4.10×10^9
k_2 [s^{-1}]	4.59×10^{-1}	4.95×10^4	5.03×10^8
$k_2 / (k_1 + k_2)$	0.0947	0.0844	0.1093

Table 2. Comparison of rate constants, k_1 , k_2 and k_3 computed by three different models, RCMC, LC-TS, and LC-mTS, and their temperature dependency (see text about the models).

T [K]	300	500	1000
k_1 (RCMC) [s^{-1}]	4.39×10^0	5.37×10^5	4.10×10^9
k_1 (LC-TS) [s^{-1}]	5.03×10^0	4.55×10^5	2.73×10^9
k_1 (LC-mTS) [s^{-1}]	9.70×10^0	9.96×10^5	7.80×10^9
k_2 (RCMC) [s^{-1}]	4.59×10^{-1}	4.95×10^4	5.03×10^8
k_2 (LC-TS) [s^{-1}]	6.28×10^{-1}	8.01×10^4	5.35×10^8
k_2 (LC-mTS) [s^{-1}]	1.24×10^0	1.59×10^5	1.60×10^9
k_3 (RCMC) [s^{-1}]	4.41×10^{-3}	1.11×10^4	4.23×10^8
k_3 (LC-TS) [s^{-1}]	2.04×10^{-3}	5.19×10^3	3.25×10^8
k_3 (LC-mTS) [s^{-1}]	4.48×10^{-3}	1.21×10^4	8.51×10^8

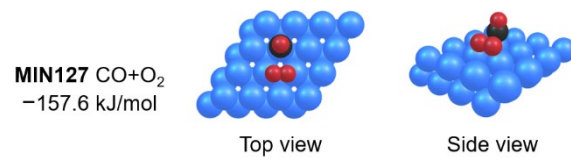


Fig. 1. Initial structure of the reaction path search. Blue, black and red ball represent Pt, C and O atom, respectively. CO molecule is adsorbed on an atop site, and O₂ molecule occupies a bridge (t-b-t) site on the Pt(111) surface. This structure is included as MIN127 in the reaction route network (see Fig. 2).

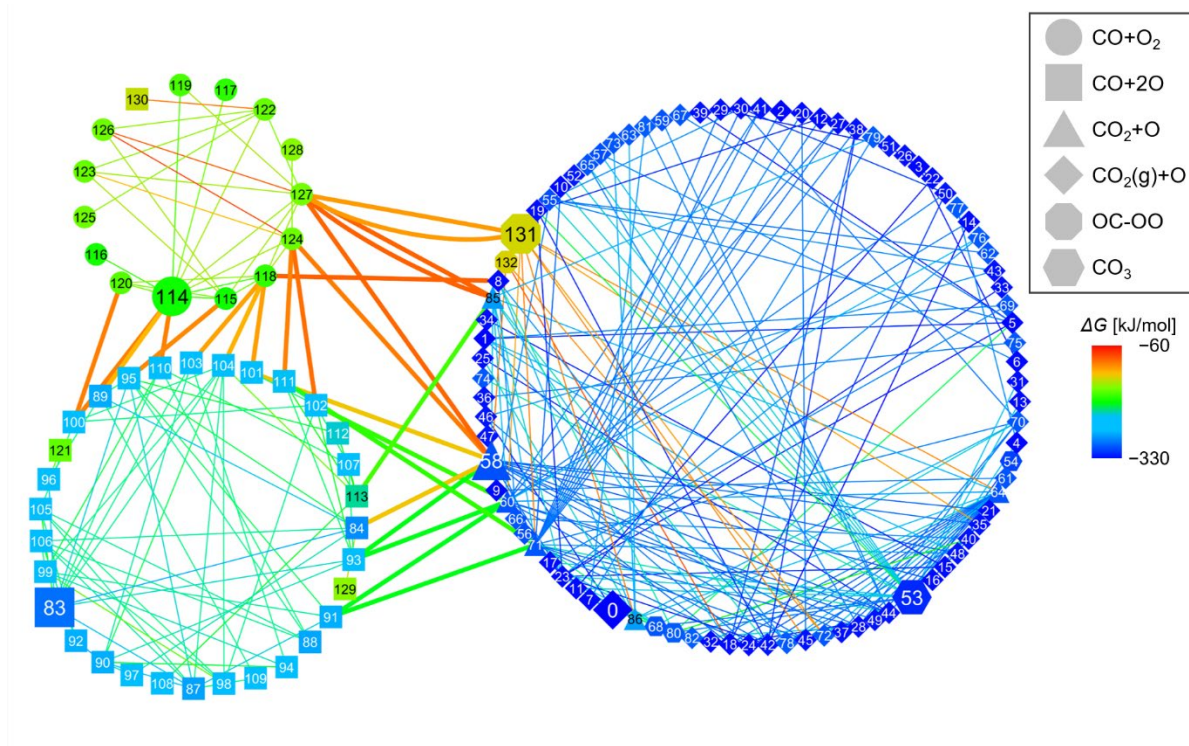


Fig. 2. Reaction route network of CO oxidation on Pt(111) surface at $T = 300$ K. Nodes and edges stand for stable structures (MINs) and connected paths, respectively. The nodes are labeled in ascending order of energy and the most stable structure is MIN0. Color of nodes and edges correspond to free energy value relative to MIN0. Shapes of the nodes represent adsorption states; the nodes are classified into six types: $\text{CO} + \text{O}_2$, $\text{CO} + 2\text{O}$, $\text{CO}_2 + \text{O}$, $\text{CO}_2(\text{g}) + \text{O}$, OC-OO , and CO_3 . The network was drawn by using Cytoscape software.⁸⁷

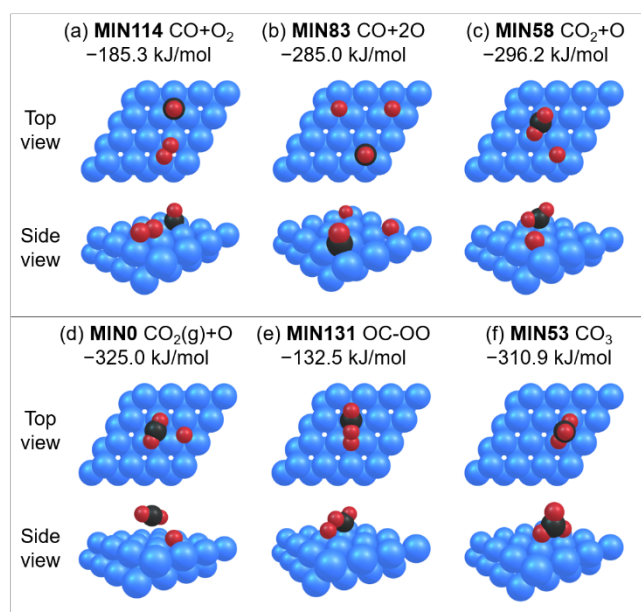


Fig. 3. Adsorption states included in the reaction route network. The most stable structure of each adsorption state is shown here. The energy values are relative free energy values to the total energy of CO(g), O₂(g), and Pt(111) surface. (a) CO molecule is adsorbed on a fcc hollow site and O₂ molecule is adsorbed on a bridge (t-b-t) site. (b) CO molecule and two O atoms are adsorbed on fcc hollow sites. (c) A bent CO₂ molecule is adsorbed. O atom is adsorbed on a fcc hollow site. (d) A linear CO₂ molecule is weakly bound by the surface. O atom is adsorbed on a fcc hollow site. (e) OC-OO complex is formed on the surface. (f) CO₃ is formed on the surface.

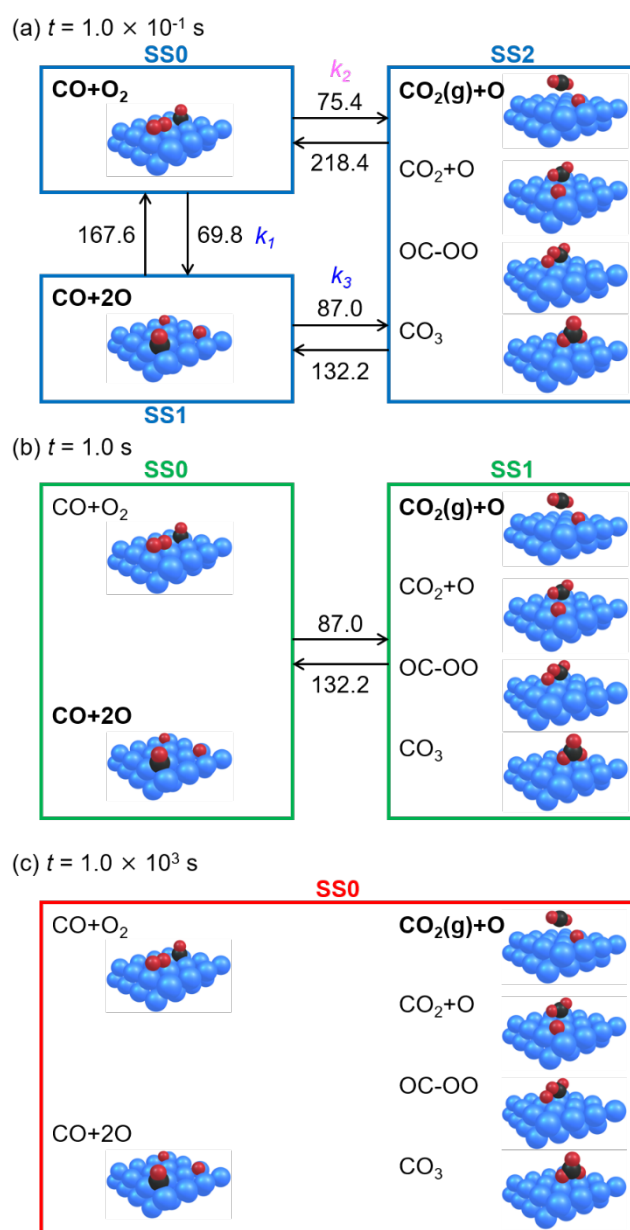


Fig. 4. Superstates given by the RCMC method with $T = 300$ K, and different timescale t . (a) At $t = 1.0 \times 10^{-1}$ s, three superstates SS0, SS1, SS2 are obtained, represented by blue boxes. The representative structure of each superstate is $\text{CO} + \text{O}_2$, $\text{CO} + 2\text{O}$, $\text{CO}_2(\text{g}) + \text{O}$, respectively. (b) At $t = 1.0$ s, two superstates SS0, SS1 are shown in green boxes. At this timescale, representative structure is $\text{CO} + 2\text{O}$ and $\text{CO}_2(\text{g}) + \text{O}$. (c) At $t = 1.0 \times 10^3$ s, only one superstate including all original states was obtained. The value in this Fig. shows relative

free energy, in the unit of kJ mol^{-1} . This value was given by calculating logarithm of off-diagonal terms of rate constant matrix from contraction results.

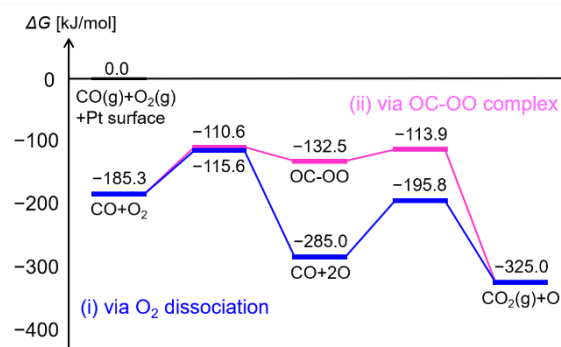


Fig. 5. Free energy profile of CO₂ formation path by the LC-TS model at $T = 300$ K. The energy values are relative free energies to the total energy of CO(g), O₂(g), and Pt(111) surface. (i) Via O₂ dissociation path is represented by blue line. The rate determining step is the second step in which a CO₂ is generated and desorbed from the surface. (ii) Via OC-OO complex formation path was represented by pink line. The rate determining step is the first step that corresponds to OC-OO complex formation process.

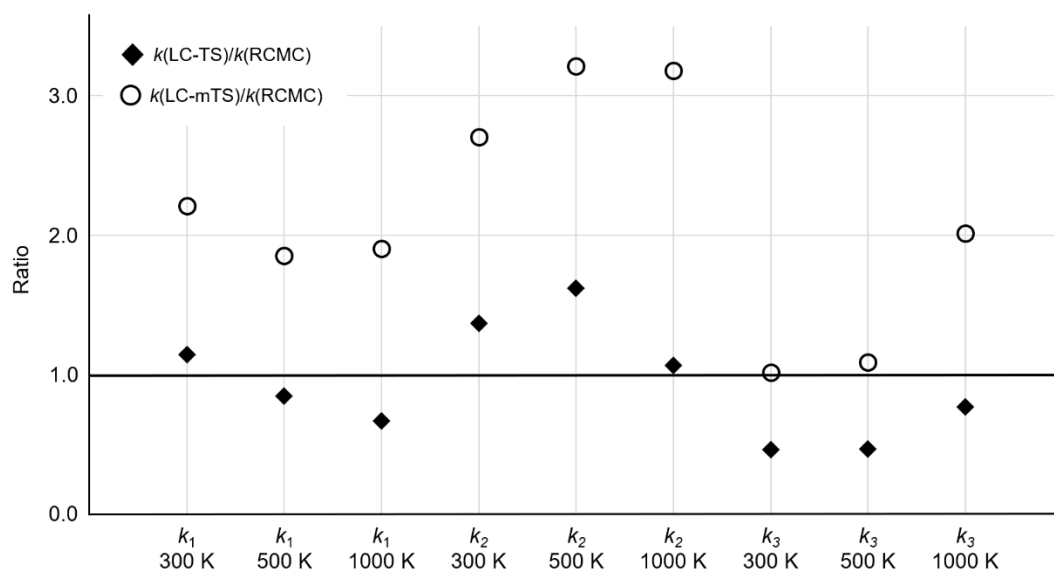
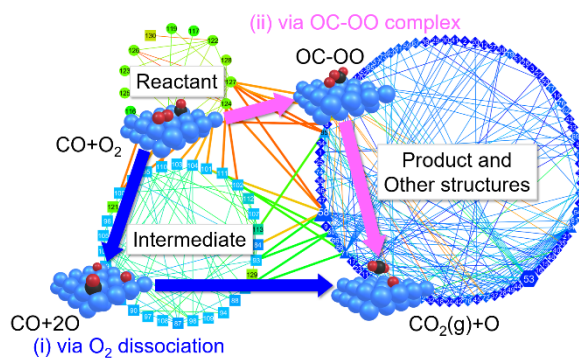


Fig. 6. Comparison of rate constants, k_1 , k_2 and k_3 computed by three different models and its temperature dependency. Ratio of $k(\text{LC-TS})$ and $k(\text{LC-mTS})$ with reference to $k(\text{RCMC})$ are shown, where $k(\text{RCMC})$ corresponds to the rate constant obtained by the RCMC, $k(\text{LC-TS})$ is the rate constant estimated from the LC-TS model, and $k(\text{LC-mTS})$ is the rate constant estimated from the LC-mTS model (see the text).

Graphical Abstract



Kinetic analysis by the rate constant matrix contraction on the reaction route network of CO oxidation on the Pt(111) surface obtained by the artificial force induced reaction reveals the impact of entropic contributions arising from a variety of local minima and transition states.